The Effect of Crack Position and Applied Force on Fatigue Delamination Behavior of GFRP's in Mixed Mode Test

Abdalla H. Alkaood[1*], Adbelhamid I. Gomma[2], Ibrahim. M. El Fahham[2], Yasser. S. Mohamed[2]

[1*,2] Department of Mechanical Engineering, Alexandria University, Faculty of Engineering, Alexandria, Egypt.

[1*] Corresponding Author's: Tel: 002/045/2862040-Mobile. 002/01220178495 – Postal code 22774 Elbohera governorate-Egypt;

E-mail address : abdallaalkaood@yahoo.com , abdallaalkaood@alexu.edu.eg

Abstract:

The present study focuses on the investigation of fatigue characteristics of fibrous composite materials with mixed mode delamination. An experimental approach was adopted, wherein a newly designed testing device was utilized to conduct fatigue tests under constant loading conditions at ambient temperatures. The tests were carried out at constant speed at 10 Hz using a variable speed drive to control the frequency. The influence of initial crack size on different forces was examined by testing rectangular specimens with fiber orientations of $[0, 90^o]_{16s}$. The specimens were fabricated using woven roving E-glass fibers and polyester resin. The test results revealed that the delamination propagation was highest in the upper quarter of the specimens' cross section under various applied forces. Additionally, the cracks in the middle and lower quarters of the cross section exhibited similar propagation behavior. The study also discussed the relationship between cycles to failure, crack length, and the impact of delamination on the fatigue life of the specimens.

Keywords: testing machine, mixed mode bending test (MMB), delamination, fatigue, crack, polyester and glass fiber.

1. INTRODUCTION

Composite materials have demonstrated significant efficacy across various engineering domains, primarily attributable to their advantageous mechanical and physical characteristics, notably their remarkable strength-to-weight ratio and resistance to corrosion and fatigue. Within composite structures, delamination is a crucial failure mode, not solely because it can lead to the fragmentation of the structure, but more importantly, because it can critically undermine the laminate's functionality, potentially rendering it ineffective in practical applications. The interface separation induced by delamination may lead to premature buckling of the laminate, increased vibration, moisture penetration, diminished stiffness, and a reduced operational lifespan due to fatigue.

In their research, the authors, **Reeder and John [1]** A test was created to apply both mode I and mode II loading on a split unidirectional laminate by utilizing a lever to exert a single load that generates mode I and mode II bending loads simultaneously on the specimen. Resulting mixed-mode bending (MMB) test underwent analysis through finite-element procedures and beam theory to determine the mode I and mode II components of strain-energy release rate (G_I and G_{II}, respectively). The comparison between the beam theory

equations and the finite-element results showed a close match, which used as a basis for selecting G_I/G_{II} test ratios and calculating the mode I and mode II components of the measured delamination toughness. **Kean Ong Low et al** [2] analysed the impact of displacement rate on the mixed-mode I/II delamination of unidirectional carbon/epoxy composites. A single leg-bending test conducted at various displacement rates, namely 1, 10, 100, and 500 mm/min. findings indicate that the mixed-mode I/II fracture toughness remains constant regardless of the displacement rate. Furthermore, the scanning electron micrographs illustrate that shear cusps are more pronounced at 1, 10, and 100 mm/min, while noticeable matrix debris is observed at 500 mm/min. In their study, **Liu and colleagues** [3] investigated the flexural damage characteristics of CFRP composites. They used a combination of both acoustic emission and X-ray micro computed tomography in their analysis. The experiment involved four specimens with varying delamination cracks, each of which was infused with 0.1wt % cellulose Nano fibers (CNFs) and subjected to a series of three-point bending tests. He concluded that for the specimens with delamination cracks near the surface, CNF samples showed no clear enhancement effect on bending strength, and its cumulative acoustic energy decreased by 28% in comparison to CFRP specimens. According to the study conducted by **L. Huo et al** [4], they carried out both experimental and numerical analyses on fully clamped rectangular carbon fiber-reinforced polymer (CFRP) laminate to investigate out-of-plane quasi-static indentations. The indentations were performed using different levels of indentation forces, and the results revealed two fundamental micro-delamination growth modes. These modes were distinguished based on the delamination fracture patterns along the 0° fiber direction and were found to be predominantly controlled by the sliding and opening micro-cracks. **Ahmed et al [5]** the investigation focused on the delamination growth in glass fiber reinforced epoxy under mix mode I/II using the MMB test method. They found the strain energy release rate is higher for mode II compared to mode I when the same load is applied. However, the strain energy decreases significantly as fatigue cycles increase in mode II tests. Additionally, the rate of crack growth decreases as the length of delamination and fiber bridging increases. The abrupt changes in the strain energy release rate are attributed to fiber bridging during fatigue tests. Moreover, the delamination growth rates are higher in tests with a higher mode I ratio. **D.H. Yoon, and colleagues** [6] conducting numerical analysis on Modes I, II, and mixed mode (I+II) interlaminar fracture, and employing Turon's methodology to derive the cohesive properties. The findings indicated that the progressive delamination analysis, utilizing Turon's methodology, can effectively forecast the interlaminar behavior of laminated composite materials with different combinations of mode mixtures. **Noh and Whitcom** [7] The investigation focused on examining the impact of various types of crack-induced delamination on the deterioration of performance. It has been asserted that the extent of crack opening is intricately linked to the decrease in stiffness of the affected interlayer. On the other hand, **Liaojun Yao et al** [8] The parameters for interpreting fatigue delamination with fibre bridging at various R-ratios were thoroughly examined, with a specific emphasis on similitude. The results suggest that, when interpreting the growth of fatigue delamination with extensive fibre bridging, it is more appropriate to utilize the strain energy release rate (SERR) applied around the crack front, rather than the total applied SERR, as a representation of similitude. **L. Huo et al.** [9] applied two consecutive out-of-plane quasi-static indentations to a fully constrained composite laminate and varied the distance between the two indentation locations through experimental and numerical studies. The results show that the delamination of the second indentation tends to spread, especially in the direction of the line from the second indentation location to the first indentation location. **Zhang et al.** [10] investigated the confinement of adjacent plies to G for stiffness reduction and delamination induced by transverse cracks in (/90°) laminates. It has been found that the stiffness reduction and energy release rate depend on the local location of the damaged

laminate. **Ogihara and Takeda [11]** employed a customized shear deceleration technique to forecast the decrease in G and stiffness of laminates caused by the development of transverse crack tip delamination. The forecast demonstrates improved agreement outcomes, particularly for laminates with thicker 90 º plies where substantial delamination takes place. **Selvarathinam and Weitsmand [12], Berthelot and Le Corre** [13] utilized a shear deceleration approach to simulate delamination triggered by transverse matrix cracks in cross laminates during environmental fatigue. The findings reveal significant delamination and decreased crack densities that emerge under conditions of immersed fatigue. **Christophe Floreani et al** [14] The research investigates the toughness and mechanical properties of unidirectional stitched glass and carbon fiber reinforced powder epoxy composites in both modes I and mixed-mode conditions. The interlaminar fracture toughness is examined in pure mode I through Double Cantilever Beam tests, along with various mode II ratios. The tensile and compressive properties are found to be similar to those of standard epoxy composites. Interestingly, both the mode I and mixed-mode toughness of these composites are higher than that of other epoxy composites, including toughened epoxies. **Salpekar and O'Brien** [15] A 3D FE analysis was employed to investigate delamination caused by matrix cracking in carbon/epoxy laminates with fiber orientations of 15° and 45˚. The study revealed that the energy release rate for localized delamination at the (45˚/-45˚) interface resulting from cracking of the (-45°) layer matrix was greater near the laminate edge than in the interior. **Mathilde Zani et al** [16] used The Finite Element (FE) models for a Double Cantilever Beam (DCB) sample, taking into account standard and multidirectional interfaces. Different initial delamination lengths were examined, showing that the delamination front shape alters at the beginning of propagation, yet stays constant afterwards and the transition zone's length for the delamination front shape is notably smaller than the specimen's width.

The objective of this experimental study is to examine the fatigue behavior of fibrous composite materials under mixed mode delamination MMB, while also analyzing the influence of initial crack size under various loading conditions and three-crack position.

2. EXPERIMENTAL WORK

2.1. Testing machine

The new introduced testing machine was designed and constructed according to ASTM International Standard D6671 as shown in **Figure 1**. The testing machine can perform mixed mode fatigue crack tests at controlled force and can rotates at a variable speed from (50 to 3000) rpm (1 to 50 Hz) through, frequency inverter (VFD). It is capable of performing fatigue loading conditions for mixed - mode delamination M_I /M_{II} at four locations (i.e. four forces can be applied) subjected to a uniform load at the end of the specimen for **mode I** and a sliding load in the middle of the specimen for **mode II**. Each specimen was affixed to the testing machine by adhering to end blocks upper and lower, then connected with pins equipped with upper and lower grabbers. The specimen is positioned on the far roller pivot at the bottom and is supported by the middle roller pivot above. Consequently, the specimen is securely held in place and prepared for testing as illustrated in **Figure 2**.

It consists of a horizontal 0.5 hp motor (H) with 3000 rpm controlled by a variable speed drive (VFD) of 1hp capacity as shown Figures 2 and 3. The motor connected to an adjustable crank (B) which gives a stroke of 0 to 20 mm by changing the eccentricity. The motor fixed with four bolts to U-beam chasses (A) of length 500 mm, width 175 mm, height 120 mm and thickness 10 mm that fabricated from material St.37. To transfer the cranks rotary motion to reciprocating motion to pull out the crack tip, a scotch yoke mechanism (C) was used with a small deep - groove ball bearing adjustable at the end of the crank and rolled inside the scotch slot. A spring arrangement (F) transmits force to the sample via a connecting rod attached to the spring to the upper grabber. The lower grabber (D) is bolted to the chassis with three Allen bolts and has the same lower dimensions as the upper grabber but differs in the middle roller support. The machine has four adjustable points and between each point different values of 40 mm. Due to the absence of welding parts, all parts of the machine can be disassembled and assembled with hand tools. The following **Figure 4** show General layout of the testing machine

Following are the main parts of the machine:
A- Chasses, B- Adjustable crank, C- Scotch yoke, D- Lower grabber, E- Upper grabber, F- Spring Arrangement G- Double cantilever specimen, H- Variable speed motor.

2.2 Materials and specimens' preparation

Woven-roving E-glass fibers and polyester resin, with trade name of "siropol 8330", were used to produce the used specimens. **Table 1** shows the properties of the tested materials [ASTM. D2150-63]. This resin was pre-promoted with Cobalt Naphthenate (6% solution), as an accelerator in percentage of 0.2 % by volume, and Methyl Ethyl Ketone (M.E.K.) peroxide as a catalyst in a percentage of 2% by volume, depending on room temperature. The volume fraction V_f, in the present work, ranges from 55% to 65% was used; because this range has proved its suitability to ensure specimens with good strength, good adhesion between fibers and matrix, and acceptable mechanical properties.

2.3 Specimen Shape and dimensions

The test specimens were uniformly rectangular, as shown in figure 5. The nominal dimensions for each specimen are outlined in Table 2, with measurements taken following the completion of the curing process. A fiber orientation of $[0, 90^{\circ}]_{16s}$ was utilized to investigate the fatigue delamination properties of GFRP composites under mixed mode bending (MMB) testing. Each specimen consisted of 16 symmetric layers and was secured to the testing apparatus by adhering to end blocks, which were then linked with pins featuring upper and lower grabbers.

3. Fatigue delamination tests

All specimens were tested under ambient conditions and constant frequency of 10 Hz. The data points were used to plot the corresponding $2a_c$-N curves on a semi-log scale, being fitted using the power law, $\mathbf{2a_c=A\ N^{B}}$ Failure was considered to occur when the cycles to failures reaches to million rpm or the crack is doubled of its original value. Tests performed to investigate the effects of initial crack length $2a_o$, applied forces **P** and crack position ratio h/t via testing rectangular specimens with $[0,90^{\circ}]_{16s}$ fiber orientation, the main test parameters are given in table 3**.** the following **Figures** 6 and 7 show the opening of initial crack and crack propagation of a specimen with ratio h/t = 0.25 under test. figures that show fatigue results in Appendix A of supplementary data.

4. Analytical study

The mixed mode-bending test (MMB) in accordance with ASTM International Standard D6671 depicted in Figure 8 consists of the Double Cantilever Beam Test (DCB), the Standard Test for Mode I Toughness, and the End Notched Flexural (ENF) Test for Mode II Toughness. A method for computing the strain energy release rate involves separating the load into Mode I and Mode II components. The pure mode stresses are employed in the toughness equations developed for the pure modes tests. Equations 1 and 2 present the strain energy release rate for Mode I, G_I and Mode II, G_{II} respectively [16], [17].

$$G_I = \frac{3P^2 2a_c^2}{z^2 E_1 h^3}\left(\frac{c+d}{2L}-1+\frac{c}{d}\right)^2 \qquad \text{Equation (1)}$$

$$\boldsymbol{G_{II}} = \frac{9P^2 2a_c{}^2}{4z^2 E_1 h^3}\left(\frac{c+d}{2L}-1-\frac{c}{d}\right)^2 \qquad \text{Equation (2)}$$

Then calculated main two parameters for MMB test, compliance coefficient and total energy release rate as represented by equations 3, 4 respectively [16], [17].

$$C = \frac{2a_c^2}{4z\,E_1 h^3}\left[8\left(\frac{c+d}{2L}-1+\frac{c}{d}\right)^2+6\left(\frac{c+d}{2L}-1-\frac{c}{d}\right)^2+\left(\frac{d\left(2L-d\right)}{L^2}\right)^2+\left(\frac{c+d}{2L}-1-\frac{c}{d}\right)^2\right]$$

Equation (3)

$$\boldsymbol{G}=\boldsymbol{G_I}+\boldsymbol{G_{II}} \qquad \text{Equation (4)}$$

Where z, d, c, h and 2L are dimensions according figure 7 for applied load arrangement in testing device. The position of the fulcrum on the lever arm is set to the mid span of the specimen, d = L= 65 mm, E_1 is the material modulus of elasticity. supplementary data file of

Appendix A show the corresponding $2a_c$-*N* fatigue curves at four initial crack length values and four applied force **P** with three crack position ratio h/t = 0.25, 0.5 and 0.75.

5. Results and discussion

Following a thorough analysis and validation of the fatigue results from the experiments, it was concluded that the power formula relationship $2a_c = AN^B$ exhibited a strong correlation with consistent values across all cases. The constants (A) and (B) are detailed in Tables 4, 5, and 6. It was noted that the $2a_c$-*N* fatigue curves, illustrated as shown in figures from figure 1 to figure 12 in supplementary data appendix A. maintained a nearly parallel alignment under varying applied loads for all initial crack values. In the case where h/t=0.25, a significant effect was observed, especially with the initial crack measuring $2a_o$=35mm, which doubled in size by the end of the experiment, indicating that a longer initial crack promotes a more rapid and straightforward progression. For h/t=0.5, a moderate effect was noted, along with a considerable displacement of the crack, particularly when the initial crack length was $2a_o$=35mm across all applied forces. In the case of h/t=0.75, a notable alteration and displacement of the crack were observed, particularly with the application of force P=323.2 N, where the initial crack length was $2a_o$=35mm. However, for the other forces applied, a consistent behavior of the cracks was observed across all instances. Among the various crack position ratios, h/t=0.25 demonstrated the highest rate of crack propagation with all applied forces when compared to h/t=0.5 and h/t=0.75. The crack propagation rates for h/t=0.5 and h/t=0.75 were similar across all applied forces. The primary distinction among the curves was the initial crack value, $2a_o$. The analysis and confirmation of the fatigue delamination constants (A) and (B), as derived from Tables 4, 5, and 6, led to the following conclusions.

i. The variation of the values of constant (A) and (B) considered and depended on the experimental conditions.
ii. Correlation factor for crack position ratio h/t=0.25, P=205.5 N and h/t=0.75, P=323.2 N is the same.
iii. The value of constant B, despite being relatively small and expressed in fractions of a hundred, cannot be regarded as a constant due to the observed variability in its values. For instance, when P is equal to 323.2N, the minimum value of B is 0.0263, whereas the maximum value reaches 0.0994. This significant disparity indicates that B should not be considered a constant value.
iv. For constant, A it found to depend on the crack location and the applied load.

5.1 Analytical results of G, C Parameters

Variations in the applied load or initial crack length during testing play a crucial role in the characterization of fatigue crack growth. The impact of the load applied during the test, along with different initial crack values, primarily affects the energy release rate and compliance coefficient parameters. These parameters are determined by Equations (1), (2), (3), and (4), which are functions of the crack length and load. The applied load values, namely P = (323.2,

264.69, 205.5, and 146.64 N), exhibit distinct differences. Notably, when the crack position ratio h/t is 0.25, the parameters G and **C** demonstrate higher values compared to crack position ratios of h/t=0.5 and h/t=0.75. The power relation and constants for the G and **C** parameters are summarized in table 7, showcasing an excellent correlation factor.

Figures 9, 10, 11, and 12 display the curves of the total energy release rate G parameter in relation to the crack length $2a_c$. A comparison of the curves reveals that, at a crack position ratio of h/t=0.25, G reaches approximate maximum values of 4500, 2700, 1700, and 750 J/m^2 with four different applied forces. These values show a significant difference compared to the values at h/t=0.5 and h/t=0.75, with an approximate difference of 4000, 2500, 1400, and 700 J/m^2 respectively. The presence of cracks in the upper part of the specimens clearly influences the behavior of this parameter. On the other hand, Figures 13, 14, 15, and 16 illustrate the compliance coefficient **C** in relation to the crack length $2a_c$. A comparison of the curves shows that at a crack position ratio of h/t=0.25, **C** reaches maximum values of approximately 550, 350, 200, and 100 mm/N. Notably, the value at h/t=0.25 is six times greater than the values at h/t=0.5 and h/t=0.75. Once again, the presence of cracks in the upper part at h/t=0.25 significantly influences this parameter.

The experimental investigation of specimens with different crack lengths revealed a clear dependence of the compliance parameter **C** and total strain energy release rate G on the crack position ratio and crack length. The previous figures illustrate this relationship. Generally, the difference between the **C** values and G values is relatively small when the crack is located at h/t=0.5 or h/t=0.75 of the sample, with a decrease of less than 25% and 35% for short cracks, and 30% and 45% for long cracks, while the applied force remains constant. However, a significant difference of about 400-500% was observed for a crack ratio of h/t=0.25 and short crack lengths, and about 800-900% for long initial crack lengths in the specimen. Based on the data from figures 9 to12, the highest applied load values for parameters total strain energy release rate G and compliance parameter **C** respectively had a significant impact on the parameters compared to the other two cases of crack position at the same length. The relationship between the parameters was governed by a power relation as shown in table 7, with the highest constant values being 0.8819 and 0.0017 for the maximum applied load case, and the lowest constant values being 0.1608 and 0.0003 for the minimum applied load case in figures 13 to 16. It can be concluded that an increase in applied load directly influenced the parameters. After examining the previous data and graphs pertaining to the primary parameters total strain energy release rate G and compliance parameter **C**, it is evident that the crack length plays a crucial role in all variables observed during the experiments. However, the impact of the crack length is intricately connected to both the magnitude of the applied force and the position of the crack in all specimens throughout the experiments. Consequently, it is regarded as an intermediary variable for the remaining experimental factors. In the Figures from figure 9 to figure 16, the parameters G and **C** were analyzed for h/t=0.25 across all specimens. It was observed that this ratio had the most significant influence on all samples, as evidenced by the values of the two parameters. This effect was consistent across various applied forces and initial crack lengths, distinguishing it from the cases where the crack was located at h/t=0.5 and 0.75. The power relation governing the

curves displayed a strong correlation factor. Therefore, it can be concluded that the h/t ratio of 0.25 had the most pronounced impact in all experiments. This difference is attributed to the second mode effect, which induces shear or sliding forces that facilitate rapid separation of layers and crack propagation. The theoretical equations (1), (2), (3) confirm this inverse relationship between the parameters and the value of h. The rapid expansion of cracks in the upper quarter of the samples under different applied forces is believed to be due to the weak strength of this region, resulting from the reduced second moment of area caused by the small width of the cracked cross section. This vulnerability makes it susceptible to external factors. This finding aligns with **[2],** which demonstrates that the crack growth rate is constant and increases with maximum applied stress and low material stiffness. The location of delamination cracks in laminates is closely related to the mechanical properties. Under low stress, the layers near the surface experience rapid faulting and a reduction in stiffness, which can compromise structural integrity and lead to premature failure. According to **[18],** this phenomenon is attributed to compressive stress exerted on the upper fiber of the specimen. As subsequent layers are compressed, the delamination continues to expand, and additional shear loads are applied to the delamination surface.

6. Conclusions:

This study introduced a new mixed-mode delamination fatigue test designed to analyze the mode mix behavior of composite materials. This test is capable of conducting mixed-mode tests with a variable M_I/M_{II} ratio, adjusting the pivot position, controlling test speed with a variable speed ranging from 0 to 50 Hz using a VFD, and modifying the applied force to the specimen by adjusting the eccentricity of the scotch yoke. The findings presented in this study can be summarized as follows:

i. The suitability of the power formula, $2a_c=AN^B$, for the present study has been proven.
ii. The constant value (A) was found to be dependent on the applied force P and the initial crack length, with reasonable correlation factors.
iii. The presence of cracks at a ratio of h/t=0.25 in the specimen resulted in a higher crack propagation rate and higher values of the parameters G and **C**.
iv. Cracks located in the upper part of the specimen lead to a reduction in stiffness and weaken its resistance to fatigue.
v. The length of the crack is considered an intermediate variable, and its effect is linked to its position and the applied load.
vi. An increase in applied load directly influenced the G and **C** parameters.

Acknowledgment

I would like to express my deepest appreciation to Prof. Dr. / Alaa El-Din Hassan Hamdy, for his unwavering support and invaluable guidance throughout our academic journey as well as his assistance in the development and design of the machine test. It is with great honor that I acknowledge his everlasting presence in our hearts.

The supplementary data is available at:

file:///C:/Users/pc/Downloads/Supplementary%20data-Alkaood%20(40-SCI-2406-9144)-1.pdf

REFERENCES:

[1] James R. Reeder and John R. Crews Jr – "Mixed-Mode Bending Method for Delamination Testing" , AIAA Journal, 28(7), pp. 1270—1276, (July 1990) https://doi.org/10.2514/3.25204

[2] Kean, O., Mahzan J., Aun N., et al. – "Displacement rate effects on mixed-mode I/II delamination of laminated carbon/epoxy composites", Polymer Testing, 108, p. 107512 (2022) - https://doi.org/10.1016/j.polymertesting.2022.107512

[3] Ran L., Gongtian Sh., Pengfei Zh., et al." Effects of cellulose Nano fibers on flexural behavior of carbon-fiber-reinforced polymer composites with delamination", Science and Engineering of Composite Materials, 30, p. 20220180 (2023). https://doi.org/10.1515/secm-2022-0180

[4] Huo L., Kassapoglou, C., Alderliesten, R.C., "A criterion for predicting delamination growth in composite laminates", Materials & Design, (2022): https://doi.org/10.1016/j.matdes.2022.111160

[5] Ahmad, S., Amjad, M.; Akram, W., et al. "Fatigue Delamination Behavior of GFRP Composites under Mixed-Mode I/II Loading", Iranian Journal of Chemistry and Chemical Engineering (IJCCE), 42 (10), (2023). https ://doi.org/10.30492/ijcce.2023.562972.5621

[6] Yoon, D.H., Lee, S.R., Kim, J.H. "Determination and evaluation of cohesive element parameters for the progressive delamination analysis",Materialwiss. Werkstofftech., 53(4), pp. 485–493 (2022) - https://doi.org/10.1002/mawe.202100359

[7] Noh J. and Whitcom J., "Effect of delaminations on opening of transverse matrix cracks", Journal of Composite Materials, 39(15), pp. 1353-1370 (2005). https://doi.org/10.1177/0021998305050427

[8] Liaojun Y., Mingyue C., Zhangming L., et al. "A proposal for similitude in characterizing fatigue delamination behavior with fibre bridging of carbon-fiber reinforced polymer composites" ,Engineering Fracture Mechanics, 295, p. 109756, 23 January (2024). https://doi.org/10.1016/j.engfracmech.2023.109756

[9] Huo, L., Kassapoglou,C. Alderliesten, R.C. "Influence of neighboring damage on delamination growth in multiple indented composites", Materials & Design 227, p.111723, (2023). https://doi.org/10.1016/j.matdes.2023.111723

[10]Zhang, J.Q., Fan, J.H., Herrmann, K.P., “Delamination induced by constrained transverse cracking in symmetric composite laminates” International Journal of Solids and Structures, 36 (6), pp. 813-846 (1999). https://doi.org/10.1016/S0020-7683%2897%2900325-9

[11] Ogihara, S., Takeda, N., “Interaction between transverse cracks and delamination during damage progress in CFRP cross-ply laminates”, Composites Science and Technology, 54 (4), pp. 395-404 (1995). https://doi.org/10.1016/0266-3538(95)00084-4

[12] Selvarathinam, A.S, Weitsman, Y.J., “A shear-lag analysis of transverse cracking and delamination in cross-ply carbon-fiber/epoxy composites under dry, saturated and immersed fatigue conditions”, Composites Science and Technology, 59 (14), pp. 2115-2123 (1999) https://doi.org/10.1016/S0266-3538(99)00069-X

[13] Berthelot, J.M., Le Corre, J.F. “A model for transverse cracking and delamination in cross-ply laminates”, Composites Science and Technology, 60 (7), pp. 1055-1066. Berthelot, (2000) http://dx.doi.org/10.1016/S0266-3538(00)00006-3

[14] Christophe F., Colin R. , Parvez A. , et al. “Mixed-Mode Interlaminar Fracture Toughness of Glass and Carbon Fibre Powder Epoxy Composites for Design of Wind and Tidal Turbine Blades”, Materials, 14, p. 2103 (2021). https://doi.org/10.3390/ma14092103

[15] Salpekar, S.A., OBrien, T.K., Shivakumar, K.N., “Analysis of local delaminations caused by angle ply matrix cracks”, Journal of Composite Materials, 30 (4), pp. 418-440. (1996) https://doi.org/10.1177/002199839603000401

[16] Mathilde Z., Daniele F., Anita C., et al. “A consistent energy-based cohesive zone model to simulate delamination between differently oriented plies”, Composite Structures, 282, p.115042 (2022). https://doi.org/10.1016/j.compstruct.2021.115042

[17] Reeder, J.R. “Refinements to the mixed-mode bending test for delamination toughness”. , Journal of Composites Technology & Research, 25 (4), pp. 191-195. (2003) http://dx.doi.org/10.1520/CTR10961J

[18] Qin R., Zhou W., Han KN., et al., “Near-surface delamination induced local bending failure of laminated composites monitored by acoustic emission and micro-CT”, J Mater Sci., 56(54), p. 19936–54 (2021). https://doi.org/10.1007/s10853-021-06513-w

Appendix (A) contain figures 9- to 20 in text and with numbers of 1-12 in appendix

Biographies

Abdalla H. Alkaood , corresponding author He is an engineer specializing in rotating machinery and a graduate of mechanical engineering department from the Faculty of Engineering at Alexandria University 2005, Egypt. He possesses a Master of Science degree in Applied Mechanics 2016 and is currently in the process of completing his PhD at the same faculty. His interests lie in mechanical design, with a particular focus on rotating machinery, Applied Mechanics and modelling &simulation.

Corresponding Author's: Tel: 002/045/2862040-Mobile: 002/01220178495 – Postal code 22774 Elbohera governorate - Egypt.

E-mail address: abdallaalkaood@yahoo.com , abdallaalkaood@alexu.edu.eg

Adbelhamid I. Gomma is an Emeritus professor of Mechanical Engineering Department-faculty of engineering –Alexandria University –Egypt;BSc (June1967),(MSc(1974) from Alexandria university. PhD 1980 universit' de Bordeaux 1, France. He has more than 50 years of experience in teaching and research with interests in Modelling and Simulation-Optimization-Tribology-machine design. (Author's Phone: 002/01001071968, Email: Abdelhamid-gomaa@alexu.edu.eg)

Ibrahim. M. El Fahham Professor in Mechanical Engineering Department, Faculty of Engineering, Alexandria University, Alexandria, Egypt. Former Executive manager of Alexandria University Community Development Center.

Councilor for the president of Borg Al Arab Technological University and former Dean of The Faculty of Industrial and Energy Technology.

B. Sc. And M. Sc. From Faculty of Engineering, Alexandria University (1986, 1991), Ph.D. from Ecole Polytechnique of Montreal (1998), His research interests Applied Mechanics - Tribology – Renewable Energy- Polymers

(Author's Phone: 002/01005010128; E-mail: ibrahim.elfahham@alexu.edu.eg)

Yasser. S. Mohamed is professor of Mechanical Engineering Department- faculty of engineering –Alexandria –Egypt; BSc, MSc and PhD 2011 from Alexandria University. He has been an active researcher with interests in Applied Mechanics, Mechanical Design, and Materials Science.

(Author's Phone: 002/01001303831; E-mail: yasser.saad@alexu.edu.eg)

List of figures of paper

List of figures of Appendix A

List of tables

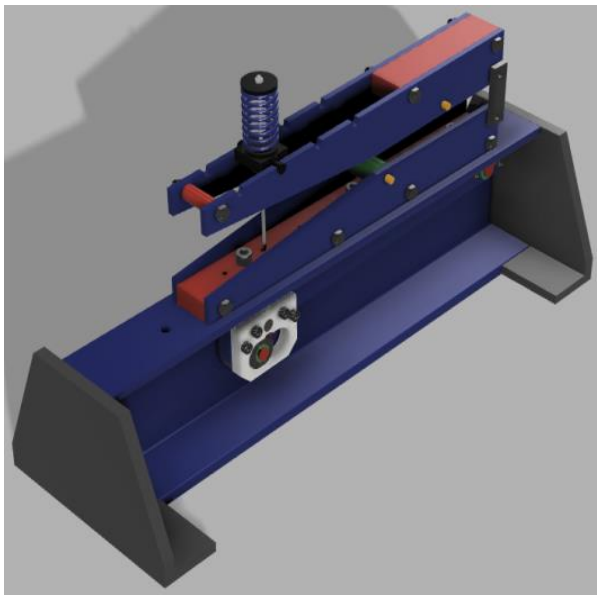

Figure 1 Mixed mode fatigue crack testing machine

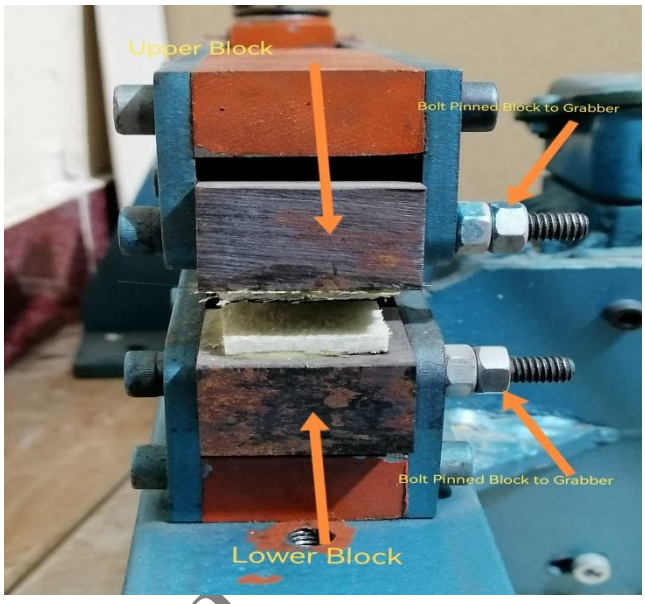

Figure 2 Specimen loaded to machine

Figure 3 Testing machine with VFD motor photo

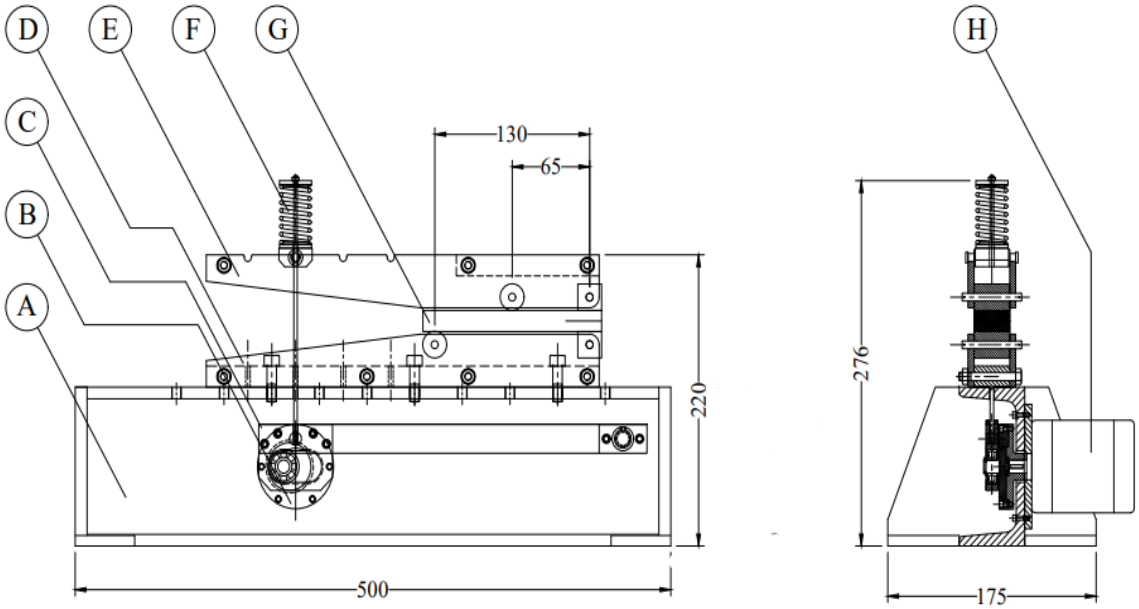

Figure 4 General layout of the testing machine

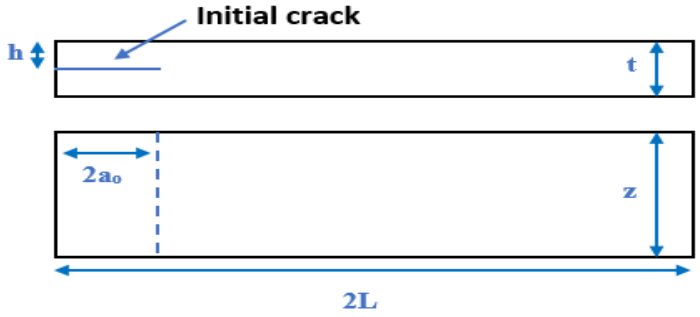

Figure 5 specimen outline

Figure 6 opening initial crack for the specimen

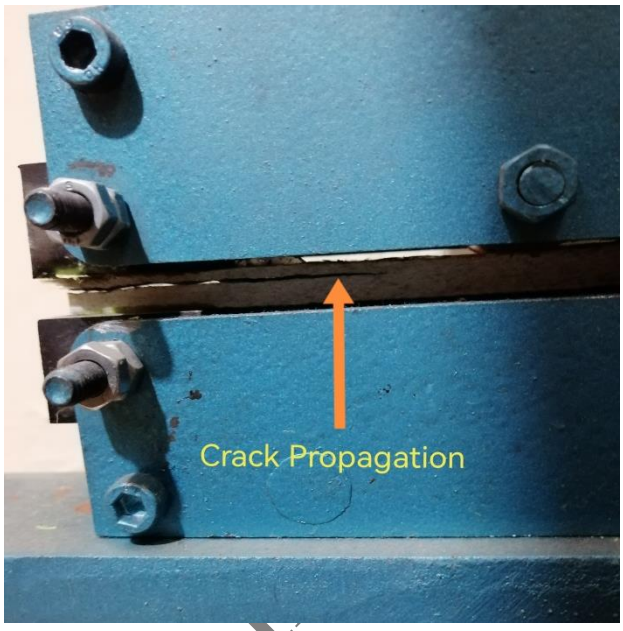

Figure 7 crack propagation for the specimen

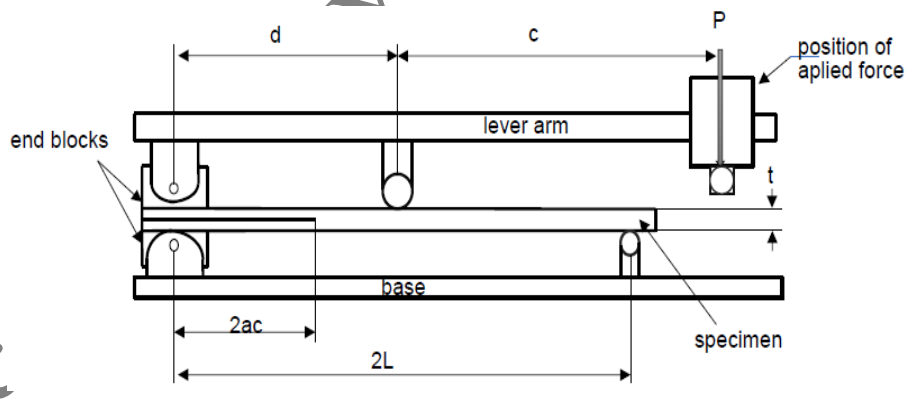

Figure 8 Mixed-mode bending test MMB

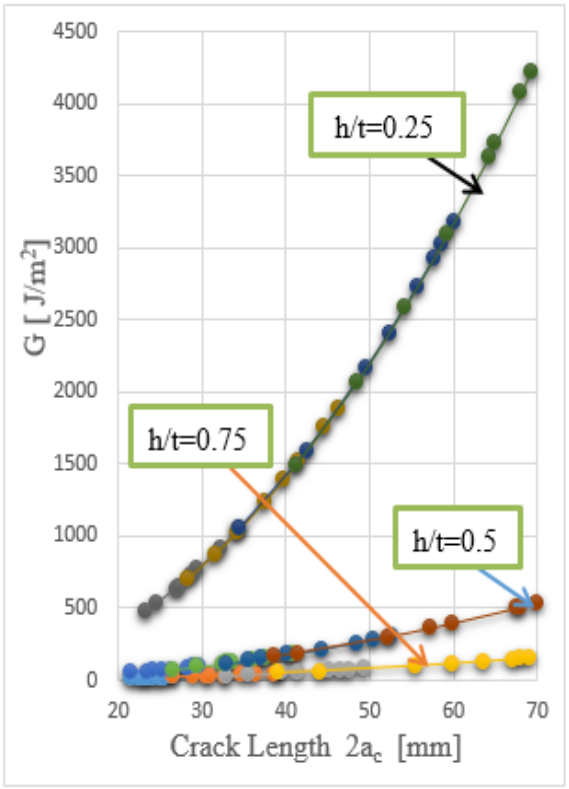

Figure 9 **G**-$2a_c$ curve at P=323.2 N

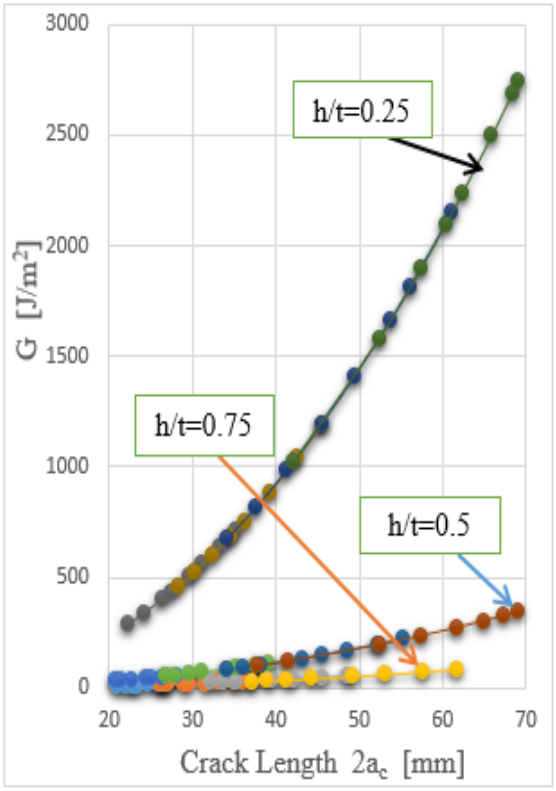

Figure 10 **G**-$2a_c$ curve at P=264.69 N

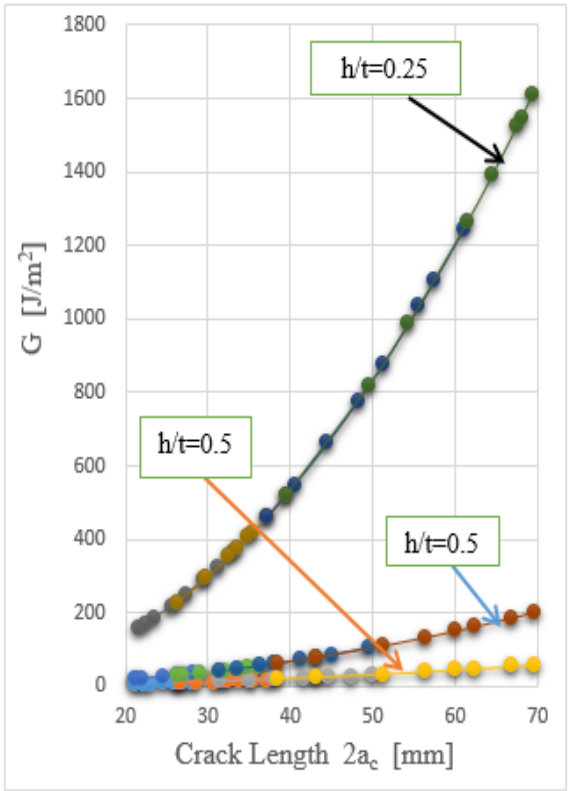

Figure 11 **G**-$2a_c$ curve at P=205.5 N

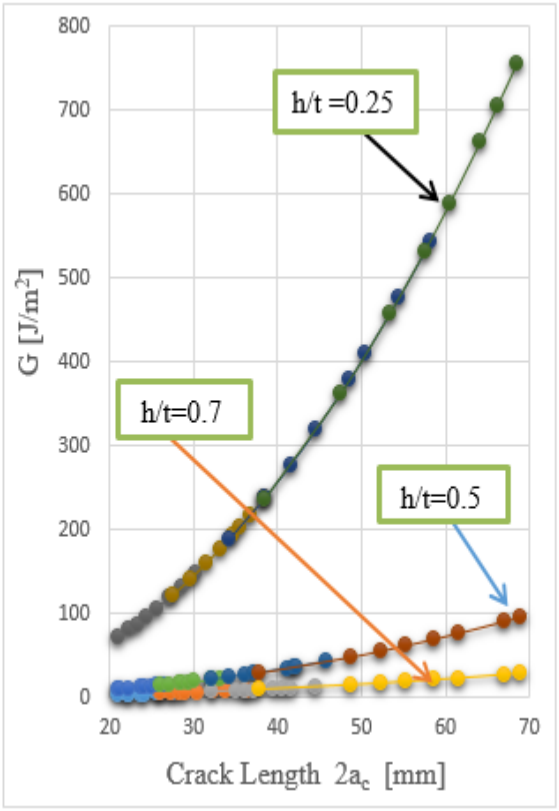

Figure 12 **G**-$2a_c$ curve at P=146.64 N

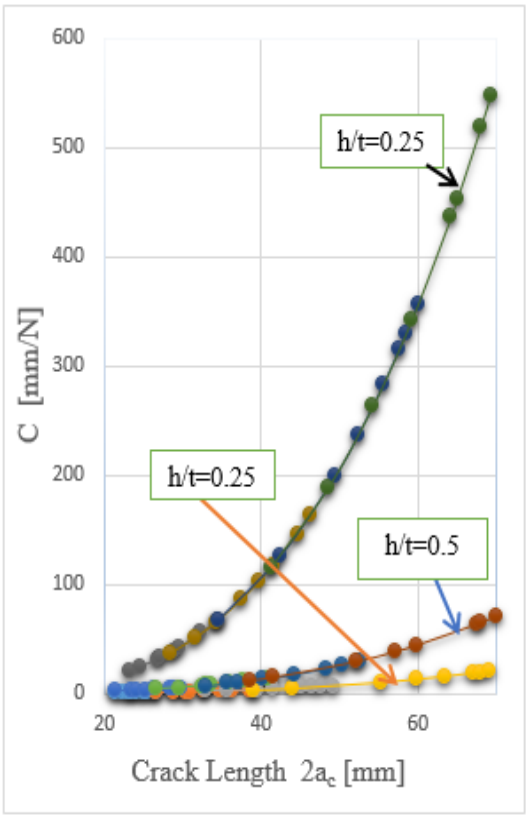

Figure 13 **C**-2a$_c$ curve at P=323.2 N

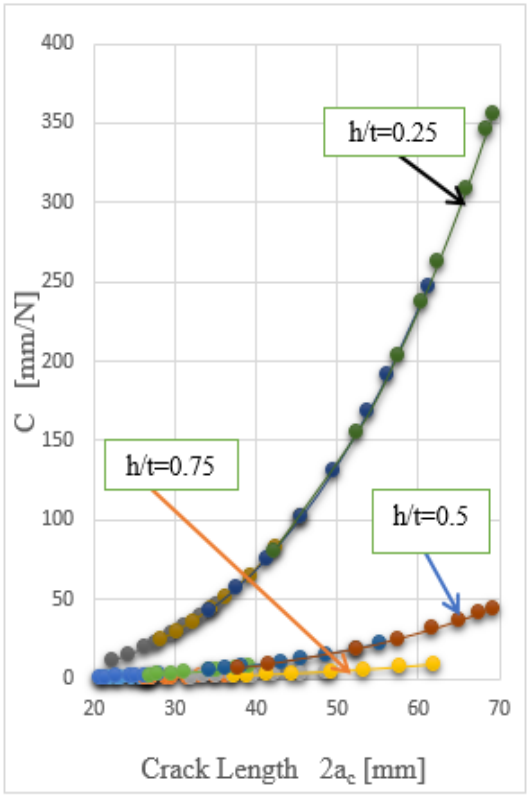

Figure 14 **C**-2a$_c$ curve at P=264.69 N

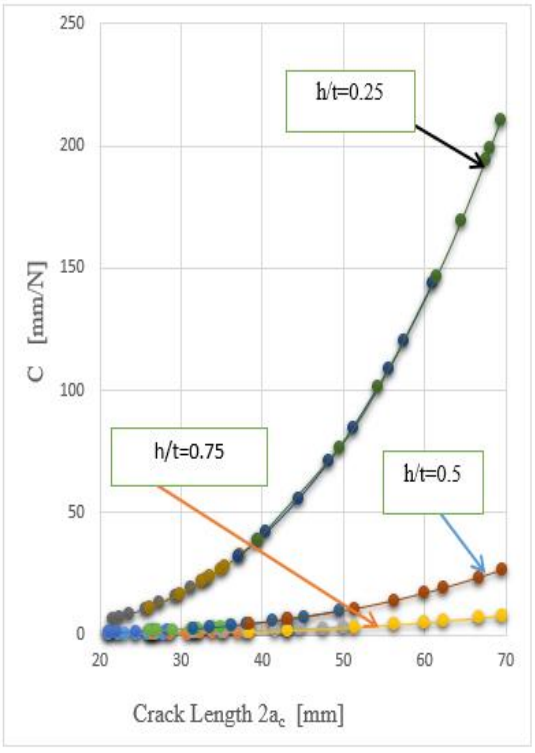

Figure 15 **C**-2a$_c$ curve at P=205.5 N

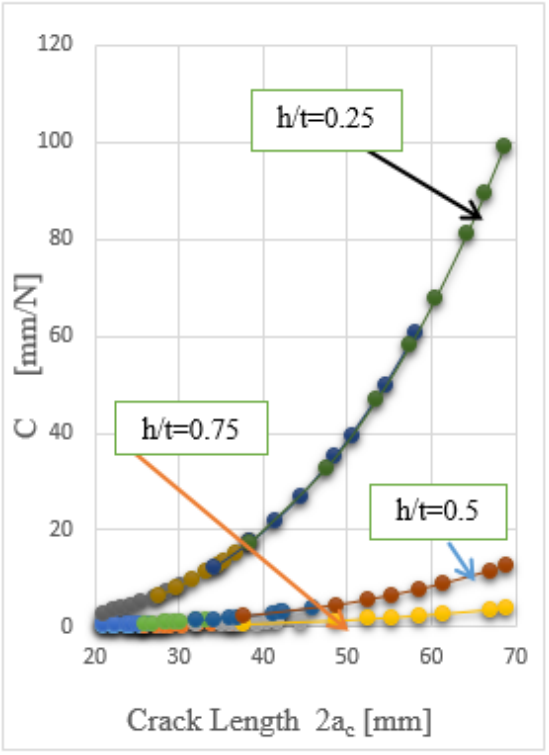

Figure 16 **C**-2a$_c$ curve at P=146.64 N

Table 1 Properties of used materials

Woven-roving E-glass fiber		**Polyester**	
Property	**value**	**Property**	**value**
Density	2551 kg /m^3	Density	1161.3 kg / m^3
Tensile strength	3.45 GPa	Gel time at 25° C	20 min.
Average mass / area	600 gm / m^2	Viscosity	0.45 Pa.s
Average thickness	0.69 mm	Percentage of Styrene	40 %
Weave	plain	Trade name	Siropol 8330

Table 2 Specimens Dimensions

Dimensions [mm]	**GFRE specimen , ±0.2 mm**
Thickness, t	12
Width, z	25
Total length, 2L	160
Initial crack length,$2a_o$	20 , 25 , 30 and 35
Crack position ratio, h/t	0.25, 0.5 and 0.75

Table 3 main parameters in test

Test parameters	units	values			
P	N	323.2	264.69	205.5	146.64
$2a_o$	mm	20	25	30	35
h/t	----	0.25	0.5	0.75	------

Table 4 Constants A, B for h/t = 0.25

P=323.2 N				**P=264.46 N**			
$2a_c$	**A**	**B**	R^2	**$2a_c$**	**A**	**B**	R^2
20 mm	15.782	0.0495	0.8254	**20 mm**	13.594	0.0572	0.7932
25 mm	17.002	0.0676	0.9194	**25 mm**	17.902	0.0551	0.7945
30 mm	19.14	0.0845	0.9802	**30 mm**	20.388	0.0745	0.9001
35 mm	21.251	0.0895	0.9398	**35 mm**	25.664	0.0729	0.9709
P=205.5 N				**P=146.64 N**			
$2a_c$	**A**	**B**	R^2	**$2a_c$**	**A**	**B**	R^2
20 mm	12.808	0.0626	0.9086	**20 mm**	14.602	0.0464	0.8146
25 mm	18.209	0.0519	0.9563	**25 mm**	19.798	0.0443	0.9267
30 mm	21.963	0.0684	0.9041	**30 mm**	20.121	0.0698	0.8926
35 mm	23.39	0.0804	0.9736	**35 mm**	22.185	0.0795	0.9843

R^2 is a Correlation factor

Table 5 Constants A, B for h/t = 0.5

P=323.2 N				P=264.46 N			
$2a_c$	A	B	R^2	$2a_c$	A	B	R^2
20 mm	15.517	0.0435	0.8791	**20 mm**	14.917	0.0419	0.8696
25 mm	18.056	0.0526	0.8887	**25 mm**	17.635	0.0521	0.8277
30 mm	19.745	0.0648	0.8269	**30 mm**	20.253	0.0656	0.8298
35 mm	17.184	0.1031	0.8846	**35 mm**	16.422	0.1044	0.8816
P=205.5 N				**P=146.64 N**			
$2a_c$	A	B	R^2	$2a_c$	A	B	R^2
20 mm	14.817	0.0431	0.8155	**20 mm**	16.072	0.0329	0.8591
25 mm	18.198	0.0459	0.8848	**25 mm**	20.552	0.0302	0.7992
30 mm	19.944	0.0583	0.8469	**30 mm**	22.412	0.0466	0.8596
35 mm	19.02	0.0938	0.8946	**35 mm**	18.501	0.0935	0.9226

R^2 is a Correlation factor

Table 6 Constants A, B for h/ t = 0.75

P=323.2 N				P=264.46 N			
$2a_c$	A	B	R^2	$2a_c$	A	B	R^2
20 mm	17.577	0.0263	0.8393	**20 mm**	15.567	0.0388	0.8848
25 mm	18.649	0.0467	0.8479	**25 mm**	17.938	0.0511	0.8972
30 mm	21.228	0.0582	0.9473	**30 mm**	21.184	0.0603	0.8634
35 mm	18.479	0.0994	0.9511	**35 mm**	16.74	0.1041	0.8956
P=205.5 N				**P=146.64 N**			
$2a_c$	A	B	R^2	$2a_c$	A	B	R^2
20 mm	15.758	0.0382	0.8985	**20 mm**	16.201	0.0336	0.8061
25 mm	19.495	0.0423	0.905	**25 mm**	18.784	0.0409	0.7589
30 mm	19.878	0.0619	0.931	**30 mm**	23.853	0.0401	0.8663
35 mm	19.01	0.0926	0.9172	**35 mm**	21.999	0.0795	0.9312

R^2 is a Correlation factor

Table 7 power relation for **C**, **G** parameters

Power law P=323.2 N				Power law P=264.46 N			
parameter	h/t	power relation	R^2	parameter	h/t	power relation	R^2
C	0.25	$C=0.0017(2a_c)^3$	1	**C**	0.25	$C=0.0006(2a_c)^3$	1
	0.50	$C=0.0002(2a_c)^3$	1		0.50	$C=8E\text{-}05(2a_c)^3$	1
	0.75	$C=6E\text{-}05(2a_c)^3$	1		0.75	$C=2E\text{-}05(2a_c)^3$	1
G	0.25	$G=0.8819(2a_c)^2$	1	**G**	0.25	$G=0.3348(2a_c)^2$	1
	0.50	$G=0.1102(2a_c)^2$	1		0.50	$G=0.0414(2a_c)^2$	1
	0.75	$G=0.0327(2a_c)^2$	1		0.75	$G=0.0124(2a_c)^2$	1
Power law P=205.5 N				Power law P=146.64 N			
parameter	h/t	power relation	R^2	parameter	h/t	power relation	R^2
C	0.25	$C=0.0011(2a_c)^3$	1	**C**	0.25	$C=0.0003(2a_c)^3$	1
	0.50	$C=0.0001(2a_c)^3$	1		0.50	$C=4E\text{-}05(2a_c)^3$	1
	0.75	$C=4E\text{-}05(2a_c)^3$	1		0.75	$C=1E\text{-}05(2a_c)^3$	1
G	0.25	$G=0.5752(2a_c)^2$	1	**G**	0.25	$G=0.1608(2a_c)^2$	1
	0.50	$G=0.0719(2a_c)^2$	1		0.50	$G=0.0201(2a_c)^2$	1
	0.75	$G=0.0213(2a_c)^2$	1		0.75	$G=0.006(2a_c)^2$	1

R^2 is a Correlation factor